AIP | Review of Scientific Instruments

Voltage preamplifier for extensional quartz sensors used in scanning force microscopy

Ireneusz Morawski, Józef Blicharski, and Bert Voigtländer

Citation: Rev. Sci. Instrum. **82**, 063701 (2011); doi: 10.1063/1.3594103
View online: http://dx.doi.org/10.1063/1.3594103
View Table of Contents: http://rsi.aip.org/resource/1/RSINAK/v82/i6
Published by the American Institute of Physics.

Voltage preamplifier for extensional quartz sensors used in scanning force microscopy

Ireneusz Morawski,[1,2] Józef Blicharski,[3] and Bert Voigtländer[1]
[1]*Institute of Bio- and Nanosystems and JARA-FIT Fundamentals of Future Information Technology, Forschungszentrum Jülich, 52425 Jülich, Germany*
[2]*Institute of Experimental Physics, University of Wrocław, pl. M. Borna 9, 50-204 Wrocław, Poland*
[3]*Department of Automatics and Robotics, AGH University of Science and Technology, Al. Mickiewicza 30, 30–059 Kraków, Poland*

(Received 21 March 2011; accepted 5 May 2011; published online 2 June 2011)

Extensional-mode quartz resonators are being increasingly used as force sensors in dynamic scanning force microscopy or atomic force microscopy (AFM). We propose a voltage preamplifier in order to amplify the charge induced on quartz electrodes. The proposed solution has some advantages over the typically used current-to-voltage converters. First, the gain does not depend on the inner parameters of the quartz resonator, which are usually unknown for the specific resonator and may even vary during the measurement. Second, with such an amplifier a better signal-to-noise ratio can be achieved. Finally, we present AFM images of the Si(111) and the SiO_2 surfaces obtained by the voltage preamplifier with simultaneously recorded tunneling current. © *2011 American Institute of Physics*. [doi:10.1063/1.3594103]

I. INTRODUCTION

High gain preamplifiers are necessary to detect low-level electric signals occurring in scanning probe microscopy. The so-called current-to-voltage converter (IVc) (Ref. 1) is in common use for both measured signals, i.e., tunneling current, and also in order to detect the charge induced at quartz sensors, e.g., Refs. 2 and 3, which are used in scanning force microscopy.[4] Although the use of a IVc is well suited for measuring tunneling current, the same circuit can be less appropriate for detecting signals from a quartz sensor; therefore, a one-stage voltage amplifier (VVa) is proposed in this work.[1] As we will show, the advantage of the latter arises from the fact that the utilized frequency of the quartz resonator (usually >10 kHz up to MHz) is much higher than the tunneling current bandwidth (usually in the order of few kHz at 10^9 V/A of the transresistance).

In the following, we consider an extensional-mode quartz crystal (also called needle sensor,[2,3,5–8] or KolibriSensor™ (Refs. 9 and 10)), which is excited electrically onto one electrode at a frequency close to the resonance frequency. The other electrode serves as an input signal for the preamplifier. The extensional resonators are characterized by their small size (a few millimeters in length), an oscillation proceeding along the quartz needle at the high resonance frequency (above 0.5 MHz), and a high effective spring constant, about 0.7 MN/m and 1 MN/m, for the 640 kHz and 1 MHz eigenfrequency, respectively,[11] Fig. 1(a). The needle has two Au-plated electrodes, which allows for an electric excitation by applying the ac (alternating current) driving signal to one electrode and electric detection from the other. The ac signal induces a longitudinal oscillation of the needle by the (inverse) piezoelectric effect. The detection of that vibration is obtained due to the piezoelectric effect as well. The mechanically oscillating needle induces charge by the piezoelectric effect, and in turn, current from the second electrode, which is amplified by the preamplifier. In order to measure an interatomic force as well as tunneling current a sharp conductive tip is attached to the top of the needle.[12] It can be a thin tungsten tip or a Si cantilever, as shown in Figs. 1(b) and 1(c). The preamplifier feds a frequency demodulator unit,[13–15] which detects an eigenfrequency shift arising from the interatomic net force[16,17] between the tip apex and the sample.

In this paper, we present experimental data obtained by the extensional-mode quartzes with eigenfrequency 640 kHz and 1 MHz; however, theoretical consideration and calculations presented here are extended to include tuning fork-type resonators as well. Although they are mostly excited by a piezoactuator in many applications,[14,18] recent investigations show the realizability of electric self-actuating and self-sensing control in case of the tuning fork[19–21] and even for the quartz cantilever.[22]

II. ELECTRONICS SETUP

A circuit of a IVc containing a quartz resonator X is shown in Fig. 2(a). Such a solution has a few disadvantages as will be outlined in the following. The amplification varies from one resonator to another because the properties of the quartz sensor, which determine its impedance enter directly into the gain arm of the preamplifier. This means that the actual gain for particular oscillators remains unknown. Moreover, for the case of a high eigenfrequency as well as a high value of the resistance R_f, the reactance X_f, which originates from the parasitic capacitance C_f, becomes dominant in the feedback loop arm of such an amplifier. This results in a decrease of the gain at the desired operating frequency, which is usually the serial quartz eigenfrequency f_s. This effect can be minimized by using various electronics designs, such as a resistor network, a compensated capacitor,[23] the double amplifying stages,[24] a bridge circuit,[25] or the feedback active parts.[26,27] Nevertheless, they introduce additional noise and

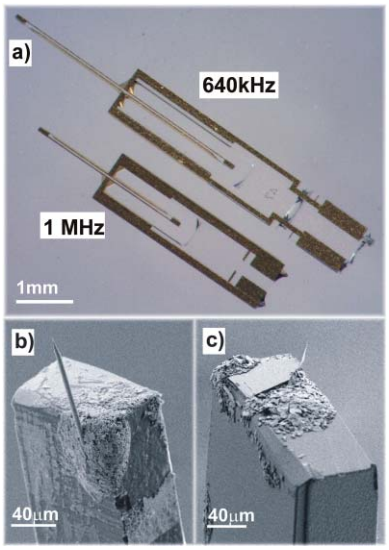

FIG. 1. (Color online) (a) An optical view of the 640 kHz and 1 MHz quartzes; the needle dimensions taken from Ref. 31: (2.18 × 0.18 × 0.09) mm^3 and (1.53 × 0.18 × 0.09) mm^3, respectively. (b) The SEM image of the needle top with an attached tungsten tip of about 5 μm diameter on the 1 MHz quartz and (c) a Pt-plated Si cantilever on the 640 kHz quartz.

the precisely determined values of passive parts are often required. In order to avoid a gain reduction as well as a complex design, we propose a one-stage voltage amplifier (VVa) to intensify the quartz signal. The circuit is shown in Fig. 2(b). The R_b and R_f resistors create a gain arm, while the quartz signal is plugged into the non-inverting input of the operational amplifier (termed opamp in the following).

In order to demonstrate the merits of such a solution, we start from Fig. 3 (inset), where the so-called open-loop gain characteristic is shown for the operational amplifier OPA657,[28] which may be a suitable amplifier for high eigenfrequency resonators. Such a characteristic determines the

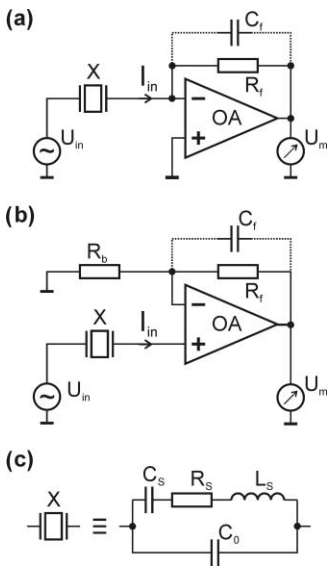

FIG. 2. (a) Electric circuit of a current-to-voltage converter, (b) a non-inverting voltage amplifier, and (c) an equivalent electric circuit of the quartz. In case of the IVc, the gain is governed by the impedance of the quartz becoming affected by its electrical parameters.

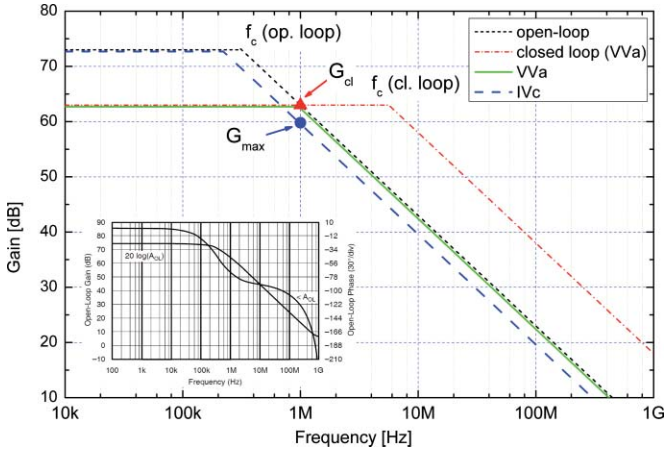

FIG. 3. (Color online) Schematic representation of the open-loop gain (dotted line), the evaluated closed loop gain obtained for the outer resistance network assuming infinite cut-off frequency of the opamp (dashed-dotted line), the resultant gain for VVa (solid line), and the resultant gain for IVc (dashed line). The characteristics are evaluated for the 1 MHz quartz. In the case of the IVc, the maximal gain G_{max} is lower than the open-loop gain value at this frequency, whereas the gain in the lower frequency range is higher than G_{max}. In the case of the VVa the gain is exactly the maximum possible value at a 1 MHz (i.e., open-loop gain) and remains constant in the lower frequency range as well. The inset shows an open-loop gain and a phase characteristic of the opamp OPA657 (Ref. 28). In this case, the maximum attainable gain value is about 63 dB (∼1400 V/V) at 1 MHz.

maximum gain, which can be reached in a circuit at a given frequency. This example is typical of a broad range of opamp types, while the exact gain values, cut-off frequencies f_c, and slopes at $f > f_c$ vary from one type to another. The cut-off frequency is determined as the frequency at which the gain falls to the 0.707 (−3 dB) of the highest value. Usually opamps have a flat characteristic from 0 Hz (direct current – dc) up to near f_c, thus the gain at f_c is well determined.

Considering the open-loop gain of the opamp shown schematically in Fig. 3 (dashed line), one can see that the maximal amplification decreases with increasing frequency above the cut-off frequency f_c. For the sake of simplicity, we draw this characteristic and the other remaining ones as having sharp corners immediately before f_c. In the following, we consider a 1 MHz needle sensor. At its operating frequency, the maximum accessible gain is about 63 dB (G_{cl} point), which is approximately three times lower than in the low frequency range (about 73 dB). On the other hand, the actual amplification of the circuits, shown in Figs. 2(a)2(b), is also determined by the external network of resistances (more generally impedances) in the appropriate arms. However, the resultant gain remains always equal to or lower than the open-loop gain at a given frequency. The low-level signals, which naturally occur in scanning microscopy sensors, require the best performance of the signal-to-noise ratio. This can be achieved if one amplification stage is utilized. Therefore, using external passive parts, which leads to the closed loop gain characteristic, two conditions should be fulfilled, namely,

(i) The cut-off frequency f_c of the closed loop gain characteristic should be higher than or equal to the working frequency (1 MHz in our case). This avoids a drop in the gain at the working frequency.

(ii) The closed loop gain (G_{cl}) should be equal to the open-loop gain at the working frequency.

If G_{cl} were higher, this would not be problematic from the operational signal amplification point of view because the total gain is limited by the open-loop gain in this case. However, this also leads to higher amplification at low frequencies ($f < f_c$) introducing an enhancement of the low frequency noise. The dot-dashed line shows the suitable characteristic. The f_c is calculated and discussed in the further text as well as the characteristics shown as dashed and solid lines.

Now, we discuss the problem of the undetermined gain in the IVc and assume for the moment that the parasitic capacitance C_f is zero and the R_f arm is purely resistive. As the equivalent electric circuit of a quartz oscillator (close to its eigenfrequencies), a four parameter model is mostly used as shown in Fig. 2(c).[29,30] It contains two parallel arms; the "motional" arm (upper part in Fig. 2(c)) consists of an ohmic resistor R_s, a capacity C_s and an inductance L_s in series. These electric quantities adequately describe the intrinsic features of the mechanical resonance in the quartz crystal bar, namely, the damping, elasticity, and the inertia, respectively. The damping can be influenced by the ambient medium as well, such as air resistance. The values of R_s, C_s, and L_s strongly depend on the type of quartz (e.g., tuning fork, extensional, or AT-cut) and their particular eigenfrequencies as well. Typical values are shown in Table I, rows 1–6.[31] The "static" arm (the lower arm in Fig. 2.) includes the capacity C_0, which is caused by the capacitance between the two electrodes as well as between the outer leads.

Although the equivalent electric circuit of the quartz resonator is quite complex, one can derive the total impedance Z_x by writing the parallel combination of the impedance Z_s in the motional arm and Z_0 in the static arm,

$$Z_x = \frac{Z_0 Z_s}{Z_0 + Z_s}. \tag{1}$$

The impedance of the electric equivalent circuit of the quartz crystal as a function of the electric quantities is then given by

$$Z_x = R_s \left[\frac{X_0^2}{R_s^2 + (X_0 + X_s)^2}\right] + iX_0 \left[\frac{R_s^2 + X_0 X_s + X_s^2}{R_s^2 + (X_0 + X_s)^2}\right], \tag{2}$$

where X_s is a reactance of the serial arm (C_s, L_s) and X_0 is a reactance of the shunt capacitor C_0.

Since the quartz sensors are used for dynamic AFM measurements, the series eigenfrequency f_s corresponding to the mechanical resonance of the quartz bar is the relevant operating frequency. The eigenfrequency f_s is characterized by a vanishing reactance of the motional arm,

$$X_s = \omega_s L_s - \frac{1}{\omega_s C_s} = 0. \tag{3}$$

Additionally, for the case of the quartz crystals considered here, the shunt capacity C_0 is relatively small, providing a large value of the shunt reactance X_0 in comparison to R_s. It is satisfied even taking into account R_s values in air (Table I. row 2.), for instance assuming $C_0 = 1$ pF, one obtains $R_s/X_0 = 0.025$ at a 1 MHz. For resonators operating in vacuum, this ratio becomes even smaller due to the lower air damping, the ratio R'_s/X_0 is shown in row 7. Applying the condition $R_s/X_0 \ll 1$ as well as the vanishing X_s, Eq. (3), the impedance of the quartz at the series resonance frequency f_s, given by Eq. (2) is simplified to

$$Z_x \cong R_s. \tag{4}$$

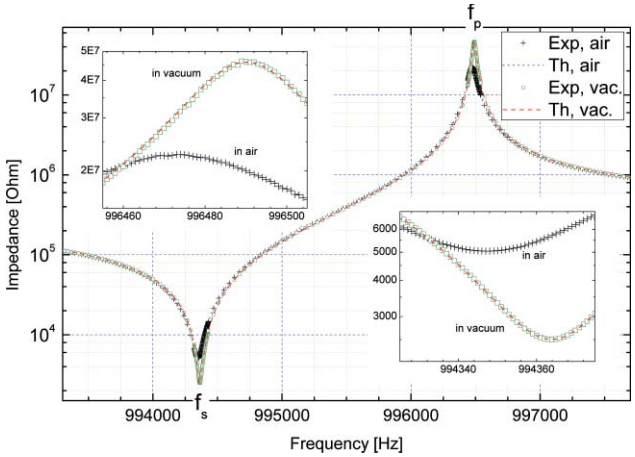

FIG. 4. (Color online) Measured and simulated modulus of the impedance Z_x of the 1 MHz quartz sensor around the serial f_s and parallel f_p resonance frequencies, symbol and line, respectively. At f_s the impedance reaches a minimum value, approximately equal to a motional resistance R_s. Lower extrinsic air damping in vacuum leads to the lower value of the R_s, right-hand insets, as well as higher impedance at f_p, left-hand inset. The impedance was measured by a Soltron 1260 gain analyzer, whereas the theoretical curves were calculated accordingly to the Appendix. Note that the simulation reflects the experimental points accurately and both are distinguished only in the magnification, shown in insets.

The impedance becomes resistive with a value approximately equal to R_s. At f_s the modulus of the Z_x reaches a minimum, which corresponds to the longitudinal mechanical resonance of the quartz bar. Figure 4 shows the measured modulus of the impedance of the 1 MHz needle sensor obtained in air and vacuum—crosses and squares, respectively. In vacuum, the lower value of R_s is caused by the lower air damping, see inset on the right-hand side. Although the value of R_s was about half as great in vacuum for the data presented here, in general that decrease holds in the range of about two to ten times. The most probable reason for this wide spread is associated with the mechanical properties of the particular sensors and also the quality of their assembling by means of the glue. The peak in the impedance at the parallel eigenfrequency f_p arises from the presence of the parallel shunt capacitance C_0.

Using the four values Z_s, f_s, Z_p, and f_p, which can be read from the experimental curve, it is possible to evaluate all the electric parameters of the motional arm, namely, C_s, L_s, R_s, and also the shunt capacitance C_0. The procedure is described in the Appendix. The initial experimental values as well as the obtained electric parameters of the investigated sensor are also shown in the Appendix. The latter are in good agreement with that given by manufacturer for the 1 MHz quartz. A slight shift of the eigenfrequencies (f_s and f_p) towards higher frequency in vacuum is observed. Quoting STATEK data, typical values of the resistance R_s in air for the remaining type

TABLE I. Electric parameters of quartz crystals operating at different resonance frequencies as well as results of calculations performed for both preamplifier circuits presented here. Values shown in rows 1–6 (except 3) were supplied by the crystal manufacturer (Ref. 31); an assumed R_s in vacuum is shown in row 3; row 7 – the ratio R_s/X_0 is estimated assuming that $C_0 = 1$ pF and at f_s; numbers in row 8 are read out from OPA657 open-loop gain characteristic (Ref. 28); rows 9–15 are calculated for IVc; and rows 16–19 are calculated for VVa, see text for details.

	Type of quartz	Tuning fork			Extensional	
1	Eigenfrequency f_s [kHz]	32.768	100	200	643	991.6
2	R_S [kΩ] in air	481	160	40	2.5	4
3	R_s in vacuum (R_s/5)	96.2	32	8	0.5	0.8
4	C_S [fF]	2.22	1.06	2.2	3.5	2.2
5	L_s [kH]	10.6	2.4	0.29	0.018	0.012
6	Q [×1000] in air	4.6	9.4	9	28.3	19.6
7	R'_s/X_0 @ f_s & $C_0 = 1$pF	0.020	0.020	0.010	0.002	0.005
8	Open-loop gain G_{ol} [dB]	73	72	71	68	63
	Current-to-voltage converter (IVc)					
9	Max gain at res. G_{max} [dB]	48.0	47.9	53.9	67.9	60
10	R_f max [MΩ] @0.90G_{max}	50.2	16.4	8.2	2.6	1.7
11	R_f max [MΩ] @0.99G_{max}	170.5	55.9	27.9	8.7	5.6
12	f_c [kHz] @0.90G_{max}	16	48	97	311	480
13	f_c [kHz] @0.99G_{max}	5	14	28	92	141
14	S/N [dB], (E_n [mV]) @0.90	36 (3.8)	35 (3.8)	38 (5.7)	41 (20)	37 (13)
15	S/N [dB], (E_n [mV]) @0.99	26 (13)	26 (13)	28 (20)	37 (35)	32 (24)
	Voltage amplifier (VVa)					
16	R_b [kΩ]	0.1	0.1	0.1	0.1	0.1
17	R_f [kΩ] @ G_{ol}	447	398	355	251	141
18	f_c [kHz] @ G_{ol}	1 780	2 000	2 250	3 170	5 640
19	S/N [dB], (E_n [mV])	43 (33)	42 (31)	54 (21)	46 (13)	43 (10)

of quartzes are shown in Table I, row 2. However, due to the reduced extrinsic damping in vacuum, an estimated five times lower values of R_s were taken into account for further calculations (row 3).

Following the result that $Z_x \cong R_s$ at f_s, it seems to be reasonable to use a IVc at the eigenfrequency f_s. However,

(i) The resistance R_s is usually not known exactly. The values given by the manufacturer apply to a packaged crystal and scatter around a mean value, while for scanning force microscopy the sensors are mounted differently and are often used in vacuum. Due to these facts, the electric parameters are only known fairly imprecisely. Specifically the Q factor and R_s are expected to vary substantially.
(ii) In scanning probe microscopy, the operational frequency usually deviates slightly from the free series eigenfrequency. This leads to a deviation of the modulus of the impedance from the minimal value, which is R_s, especially because the impedance changes rapidly close to the series resonance frequency (see Fig. 4).

The voltage amplifier proposed here avoids the problem of an unknown gain arising due to the unknown value of the impedance of the crystal at the operating frequency. In the VVa circuit, the gain is set by the resistors (R_b and R_f) in a feedback arm of the operational amplifier (Fig. 2(b)), and their impedances (resistances) are not influenced by the quartz features.

The other serious problem occurring in the case of the use of quartz resonators is the parasitic capacitance C_f parallel to the resistor R_f which originates from contacts, wires, and/or metallic paths on the printed circuit board. As will be shown, it is advisable to reduce C_f as much as possible, e.g., designing short metallic paths, nevertheless it is impossible to remove it completely. Using a surface-mounted resistor R_f and soldering it as close as possible to the opamp pins, one can reach a value of about 0.2 pF, which we use for the further calculations.

Assuming that the operational frequency is still near to the series eigenfrequency of the quartz, the transfer function H and cut-off frequency f_c for inverting (here I/V converter) amplifier can be written as follows:[32]

$$H_{IV}(\omega) = -\frac{R_f}{R_s}\frac{1}{1 + i\omega R_f C_f}, \quad f_c = \frac{1}{2\pi R_f C_f}. \tag{5}$$

The gain is derived from transfer function as follows:

$$G_{IV} = |H_{IV}(\omega)| = \frac{R_f}{R_s}\frac{1}{\sqrt{1 + \omega^2 R_f^2 C_f^2}}. \tag{6}$$

For the low-frequency range, i.e., $f < f_c$, the gain is determined by the left-hand factor, whereas right-hand factor involves a significant decrease of G_{IV} above f_c. Therefore, the gain approaches a value (G_{max}) for $R_f \to \infty$ at a given frequency, namely,

$$G_{max} = 1/\omega R_s C_f. \tag{7}$$

The open-loop gain G_{ol} of OPA657 and the values of G_{max} at $f = f_s$ are shown in rows 8 and 9 in Table I, respectively. For all cases, G_{max} is lower than G_{ol} leading to a loss of preamplifier performance, specifically for low-frequency quartzes. It is worth noting that one would expect G_{max} to decrease

with increasing frequency due to the 1/f dependence. However, the product of the eigenfrequency and the motional resistance $\omega_s R_s$ enters into Eq. (7) causing a rise of the G_{max} with frequency. In order to increase the closed loop gain G_{max}, the parasitic capacitance C_f has to be decreased. This requires great effort in the design of electric leads, and it is not possible beyond a certain level.

Evidently, the real circuit requires a finite value for R_f. We therefore introduce a coefficient k, which is defined as follows: $G_r = kG_{max}$, where G_r is the gain desired in the preamplifier circuit, with $0 \leq k < 1$. The R_f can be expressed as follows:

$$R_f = \frac{k}{\sqrt{1-k^2}} \frac{1}{\omega C_f}. \tag{8}$$

The values of R_f are shown in rows 10 and 11 for $k = 0.9$ and $k = 0.99$, respectively. The $k = 0.9$ corresponds to about the 0.9 dB decrement of gain.

Even in spite of a satisfactory maximal gain in the MHz range, the cut-off frequency quantity (see Eq. (5).) of such a circuit shows that the gain for $f < f_c$ is higher than G_{max} involving unnecessary amplification of noise below f_s. The f_c calculated for the two chosen values of k are shown in rows 12 and 13. It is seen that even for 90% of maximum gain the cut-off frequency is half that of the operational frequency. This becomes even worse if coefficient k approaches one. Such a characteristic is shown in Fig. 3. For $k = 0.99$ and 1 MHz quartz, blue dashed line, where both the problems mentioned above are readily visible. Using coefficient k, it can be conclusively seen that the increase of the desired gain by rising R_f does not lead to the expected effect, i.e., better performance of the IVc. This is caused by the relatively large value of R_s, which forces the use of a larger value of R_f. In turn the latter becomes much larger than the parallel shunt reactance of C_f. Therefore, the resultant gain is governed mainly by reactance X_f above f_c, which is lower than the working frequency f_s. On the other hand, the gain becomes larger for the low frequency range ($f < f_c$) introducing unwanted noise to the system. To avoid this latter problem, a possible solution is to use such R_f for which the gain at dc would be equal to G_{max} at operating frequency (f_s). It leads to the $R_f = 1/\omega_s C_f$ expression for R_f, equating the left-hand factor from Eq. (6) with Eq. (7). Further substituting it in Eq. (5) for f_c, the cut-off frequency $f_c = f_s$ is finally obtained, which proceeds for $k = 0.707$. Though it leads to a 3 dB decrement of the gain (relative to G_{max}) at f_s and one is the proper solution knowing the exact value of R_s, see Eq. (7), which again can be only determined approximately.

As it will now be shown, the proposed voltage amplifier avoids the problems mentioned above. The transfer function of the voltage amplifier is[32]

$$H_{VV}(\omega) = \left(1 + \frac{R_f}{R_b}\right) \frac{1 + i\omega R_b C_f}{1 + i\omega R_f C_f}, \quad R_f \gg R_b. \tag{9}$$

The condition $R_f \gg R_b$ applies because a high gain of the amplifier is demanded. This transfer function does not contain any quartz parameters, enabling a free choice of the resistances R_f and R_b. The gain of the VVa is given by

$$G = |H_{VV}(\omega)| = \left(1 + \frac{R_f}{R_b}\right) \sqrt{\frac{1 + \omega^2 R_b^2 C_f^2}{1 + \omega^2 R_f^2 C_f^2}}, \tag{10}$$

while the cut-off frequency is that already given in Eq. (5). In particular to decrease the influence of the parasitic capacitance C_f on the gain at a given working frequency, one can apply lower values of R_f and R_b. The former leads to an increase of the f_c providing a flat characteristic at $f < f_c$ with a gain well determined by external resistors.

The asymptotic analysis for $R_f \to \infty$ leads to an equation which is analogous to Eq. (7),

$$G_{max} = 1/\omega R_b C_f. \tag{11}$$

However, the resistance R_b is now not an electric parameter of the quartz and can be chosen freely, here we select $R_b = 100\ \Omega$. The corresponding values for R_f necessary in order to reach the open-loop gain are shown in row 17 in Table I. The values of R_f are two to three orders lower than in the case of IVc. The values of f_c are shown in row 18 of Table I. They are higher than the working frequency of the quartz and the cut-off frequencies of the IVc as well, leading to a flat gain characteristic in the relevant frequency range. Finally, the resultant closed loop gain characteristic of the VVa, which is estimated for the 1 MHz quartz resonator, is shown as a solid line in Fig. 3.

III. NOISE DISCUSSION

Applying noise analysis for a simple model of the circuits as well as a high value of the gain, i.e., $(1 + R_f/R_b)^2 \cong (R_f/R_b)^2$, one can derive the following expressions for the output voltage noise density:

$$\begin{aligned} e_{IV}^2 &\cong (G_{IV})^2 \left[u_n^2 + 4k_B T R_s\right] + 4k_B T R_f + (i_n R_f)^2, \\ e_{VV}^2 &\cong (G_{VV})^2 \left[u_n^2 + 4k_B T R_s + 4k_B T R_b + (i_n R_s)^2\right] + 4k_B T R_f' \\ &\quad + \left(i_n R_f'\right)^2, \end{aligned} \tag{12}$$

for a IVc and a VVa, respectively, where u_n and i_n are the input voltage noise and input current noise density of the opamp, k_B, and T are Boltzmann's constant and ambient temperature, respectively. A component $4k_B T R_s$ is the equivalent noise resistance of the quartz crystal, which is the same as the thermal noise of its motional resistance R_s.[33] Here, we establish that the value of the feedback resistance is different for the IVc and the VVa, R_f, and R'_f. As long as one can use FET opamps (here OPA657), the noise contribution associated with the input current noise i_n is significantly lower than the input voltage noise u_n and Johnson noise as well. Moreover, the thermal noise of the resistor R_f (R'_f) can be also neglected even for the large value of its resistance (gain) used in our cases. And due to the low value of R_b, its thermal noise is at least about 25 times lower than the thermal noise of R_s. The output is dominated by the worst noise in the circuit, i.e. the largest summand in this expression due to the square root of the sum of squares. The above facts lead to a simpler expression for

output noise density for both preamplifiers:

$$e_n^2 \cong G^2 \left(u_n^2 + 4k_B T R_s\right). \quad (13)$$

This result shows that dominant noise contributions are the same for both circuits and the signal-to-noise ratio at a given frequency is independent of the resistors used. However, calculating the total output voltage noise E_n for the desired bandwidth,[34] one should know that in general the FET opamp input voltage noise density and the gain do not remain constant up to working frequency f_s. A more detailed derivation, which includes the 1/f contribution of the opamp voltage input noise and the fact that the total gain is limited by the parasitic capacitance C_f, Eqs. (6) and (10), lead to the formula[35]

$$E_n^2 \cong 1.57 G_P G_{DC} \left[u_n^2 \left(\frac{f_{nc}}{f_s} \ln \frac{f_s}{10} + 1\right) + 4k_B T R_s\right]. \quad (14)$$

The parameter f_{nc} is the noise corner frequency, the left and right term in rounded brackets contains flicker noise (1/f) and white noise of the opamp contribution, respectively. An effective noise bandwidth of the first order low pass filter is taken into account, the coefficient 1.57.[34] In order to obtain a finite E_n value, the 10 Hz high pass filter is assumed, the number 10 in the Eq. (14).[35] The G_P is the gain-bandwidth product parameter of the opamp, the G_{dc} means G_{IV} or G_{VV} for dc.

In order to evaluate the total voltage noise E_n, the following parameters of the OPA657 were used $u_n = 7$ nV/$\sqrt{\text{Hz}}$, $f_{nc} = 1170$ Hz, $G_P = 230$ MHz as well as the ambient temperature $T = 300$ K. The results are shown in the brackets in rows 14, 15, and 19 for the IVc (at $k = 0.9, 0.99$) and the VVa, respectively. Higher values occur for the VVa than for the IVc at lower eigenfrequency. Nevertheless this trend undergoes a reversal for high resonance frequencies. To evaluate the performance of the given circuit, the relative signal-to-noise ratio was estimated as follows: a constant amplitude of the oscillation is established in both cases (VVa and IVc), then this amplitude is amplified with the given gain, rows 8 and 9 of Table I, respectively. In order to obtain the S/N ratio this result is divided by the product of the total voltage noise (E_n) and the input oscillation amplitude. An absolute (S/N) ratio can be evaluated knowing an actual input and output amplitude. The results are also shown in rows 14, 15, and 19. Even though the total output noise is larger for the VVa, the signal-to-noise ratio (S/N) of the VVa is higher on average by about 7 dB and 16 dB, compared to IVc with 0.9 G_{max} and 0.99 G_{max}, respectively.

Such a result is mainly affected by the larger gain at the lower frequency for the IVc (G_{dc}) in comparison with its gain at the f_s (G_{IV}). This leads to enhancement of the low-frequency noise contribution to the total output noise E_n. In the case of the VVa the cut-off frequency f_c calculated theoretically is much higher than the utilizing frequency f_s, therefore the gain remains constant over whole bandwidth. It is worth noting that, in case of IVc, the larger feedback resistance R_f leads to a two to three times higher output noise. However, the gain remains almost at the same level at f_s, the increment reaches only about 0.9 dB.

In summary, the VVa enables full control over the whole frequency-gain characteristic of the preamplifier by means of external resistors and utilization of the maximal gain accessible for the given type of opamp as well. These two facts significantly improve the signal-to-noise ratio.

Although, the numbers presented are calculated using sufficiently strict formulas, it should be remembered that such quantities as the parasitic capacitance C_f, the equivalent quartz resistivity R_s, and the opamp parameters (u_n, G_P, f_{nc}) can vary from one electronic circuit to another thus strongly affecting the finite effect. The main aim of the calculation performed above is to show the qualitative benefit of the voltage amplifier over the current-to-voltage converter by means of the quantitative elaboration.

The output of the preamplifier, a IVc or a VVa, is plugged to the next stage of the AFM electronics, i.e., the frequency demodulator, influencing the quality of the signal taken as an input signal in the topography feedback loop. The spectral noise densities of the easyPLL plus[36] frequency demodulator output signal (so-called frequency shift or detuning) are shown in Fig. 5 and were measured for the IVc and VVa preamplifiers for a 640 kHz quartz. Although, in the case of the IVc, two values of a feedback resistor were used (100 MΩ and 1 GΩ), no significant difference is visible. This is due to the low cut-off frequency, Table I, rows 11 and 12, or in other words, the gain is governed by parasitic capacitance C_f rather than R_f in a frequency range higher than f_c, see Eq. (7). The spectral noise density of the KolibriPreamp,[37,38] which is used as reference data, is shown in Fig. 5 as well. According to Refs. 4, 13, and 39 in high Q environments, the linear increase of the noise density dependence is observed, whereas the decline above about 0.9 kHz results from the built-in 1300 Hz low pass filter of the PLL demodulator. Taking into account the slope of the linear part and a mechanical oscillation $A_0 = 0.15$ nm, which was determined in a separate experiment,[12] the deflection noise of a particular preamplifier was estimated as: 1.0 fm/$\sqrt{\text{Hz}}$ for the KolibriPreamp, 4.4 fm/$\sqrt{\text{Hz}}$ for the voltage preamplifier, 8.0 and 8.3 fm/$\sqrt{\text{Hz}}$ for the IVc with the 100 MΩ and 1 GΩ feedback resistor, respectively. The measurements were performed in the final AFM/STM system, which means that the measured data include all noise sources, such as unshielded parts (e.g., needle sensor), lead wires, common grounds, etc. Nevertheless, the deflection noise density of the KolibriPreamp determined here is in good agreement with data from the manufacturer (<1.0 fm/$\sqrt{\text{Hz}}$), which leads to the conclusion that the above numbers seem mainly related to the intrinsic noise of the particular preamplifiers used in this experiment.

IV. APPLICATION

All scanning probe microscopy data presented in the following were taken by means of a needle sensor quartz with a tungsten tip attached at the top. Oscillations were detected by a voltage amplifier, while the tunneling current was transferred into voltage by a home-made current-to-voltage converter based on OPA111 opamp[28] with a 10 GΩ feedback resistor, i.e., 10^{10} V/A of the transresistance. Both circuits, the low-frequency IVc, as well as the high-frequency

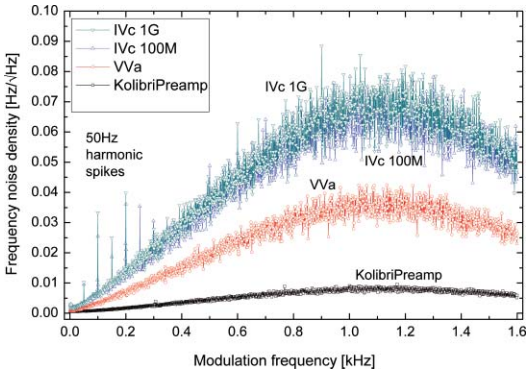

FIG. 5. (Color online) The spectral noise density of the easy PLL output signal (frequency shift) measured for: a current-to-voltage converter (Fig. 2(a)) with $R_f = 100$ MΩ and 1 GΩ, the voltage amplifier (Fig. 2(b)) as well as the KolibriPreamp (Refs. 37 and 38) as the reference preamplifier. Data were recorded *in situ* for the 640 kHz quartz at an oscillation amplitude $A_0 = 0.15$ nm and demodulator bandwidth of the1300 Hz using the HP35670A spectrum analyzer. The VVa reveals a lower level of noise than the IVc. Interestingly, in the case of IVc, harmonics of 50 Hz power line interferences arise from cross-talk of common grounds in the electronic system.

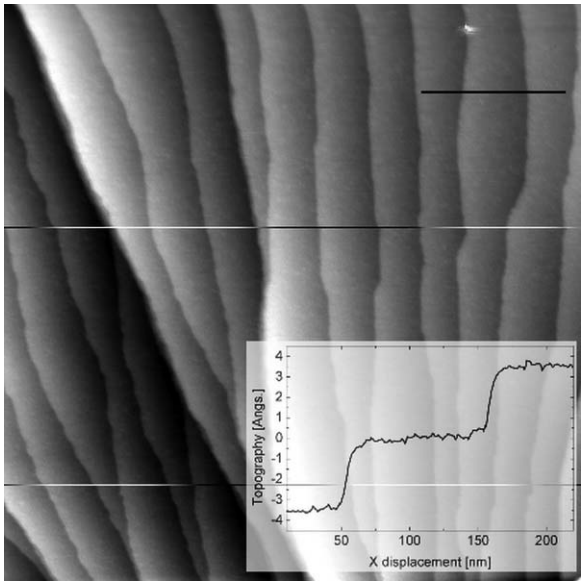

FIG. 6. The SFM scan of (0.9×0.9) μm^2 area of SiO_2 obtained with the 640 kHz needle sensor. Atomic steps are readily apparent; see profile along black line. Z-noise is observed at about 0.3 Å. Parameters of scanning: oscillation amplitude 1.2 Å, frequency shift −0.36 Hz (−0.44 fNm$^{0.5}$), demodulator bandwidth 120 Hz, scan speed 7300 Å/s, bias voltage +0.5V compensating contact potential.

VVa, were combined electrically in the manner described in Ref. 12. Such a solution provides only two leads (pins) to supply the needle sensor, which can be an advantage in some cases. The non-contact mode with constant frequency shift at the constant amplitude of the tip oscillation was applied to measure interatomic forces. In order to demodulate frequency shift, the easyPLL plus equipment was used,[36] then the voltage proportional to the frequency shift (i.e., force gradient) was supplied to the input of the Z-piezo feedback loop. The mechanical amplitude of the needle oscillation was determined using the tunneling current as the piezo-Z feedback signal.[12,40] The contact potential[2] between the sample and the tip was compensated by adjusting the applied bias voltage. Its value was determined from the maximum of frequency shift versus bias voltage parabola dependence. The Si(111) sample was prepared in the usual way, namely, a long annealing time and then repetitive flashing.

Figure 6 shows a large image (∼1 μm^2) of a SiO_2 surface on Si(111) scanned at a relatively large scan speed of about 7000 Å/s. The surface was oxidized by leaving an initially cleaned (7×7) surface for 1 h under an oxygen atmosphere of about 1 bar. Single atomic steps of about 3 Å in height can be observed at a noise level of 0.3 Å as shown in the inset. Details of the scan parameters are given in the figure caption.

A second example is the clean Si(111) surface. Due to rapid quenching after flashing the (7×7) reconstruction formed only close to the step edges, as seen by the regular pattern left from each step edge. The other part of the surface is disordered. Figure 7(a) shows the SFM topography and Fig. 7(b) the simultaneously recorded tunneling current obtained for a large area in comparison to the unit cell. The contact potential[2] was determined to be about +20 mV. During the scan the tunneling voltage was changed to different values, as indicated in Fig. 7(b), around about +10 mV. As a result, the opposite polarity of the tunneling current is obtained, while its pattern remains similar. It is worth pointing out that tunneling current varies from about −10 pA up to +10 pA. The recorded values shown in Fig. 7(b) are averaged over time by a 150 Hz low pass filter of the I/V converter. Therefore, the momentary tunneling current could even reach 100 pA. Such a high and fast modulation as well as a flow direction does not affect the VVa output signal. Although the tunneling current mean value is relatively small also at the relatively small bias voltage, the estimated lowest resistance of the tunneling gap is in the order of 0.2 GΩ, which is a reasonable

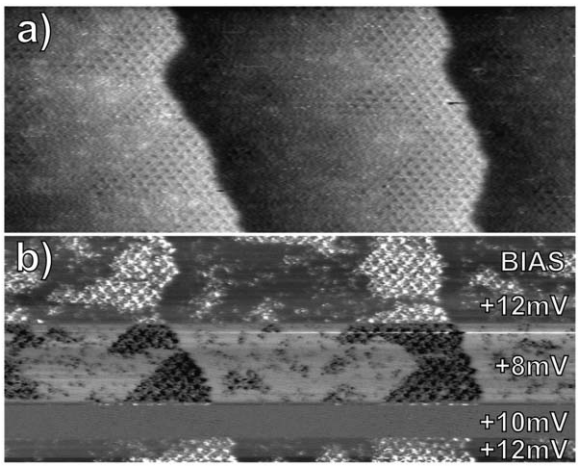

FIG. 7. (a) The SFM topography and (b) tunneling current of ordered and disordered domains on the Si(111) surface, image (100×100) nm^2 obtained by the 1 MHz needle sensor. The bias voltage was changed in the range from +12 mV to +8 mV during scanning, giving the opposite polarity of the tunneling current, bright and dark strips, respectively. Parameters of scanning: oscillation amplitude 1 Å, the frequency shift −0.32 Hz (−0.27 fNm$^{0.5}$), demodulator bandwidth 120 Hz, scan speed 1800 Å/s.

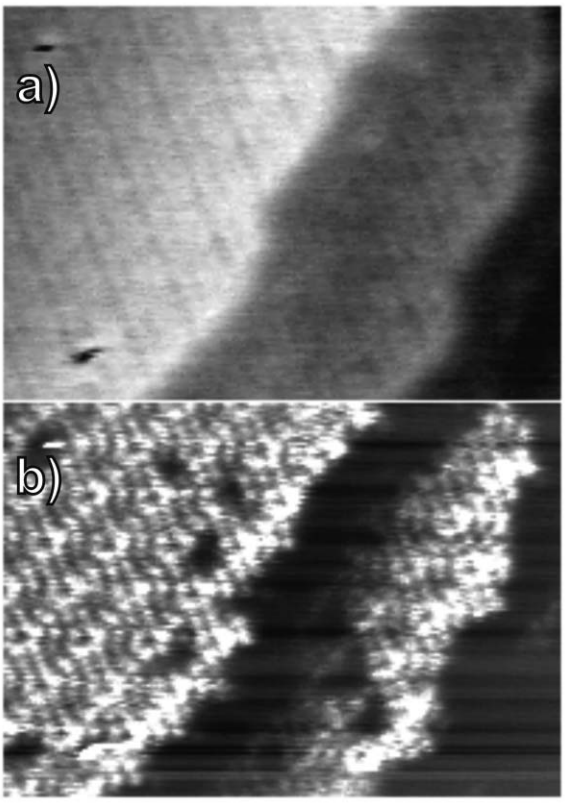

FIG. 8. (a) The SFM topography signal and (b) tunneling current of the Si(111) -7×7 domain, (25×25) nm^2 area obtained by the 1 MHz needle sensor. The +14 mV BIAS voltage provides tunneling current of up to +10 pA. Parameters of scanning: oscillation amplitude 1 Å, the frequency shift −0.21 Hz (−0.18 fNm$^{0.5}$), demodulator bandwidth 120 Hz, scan speed 900 Å/s.

value in comparison with STM measurements. The Si(111) $-(7 \times 7)$ domains are well reflected by modulation of both the tunneling current and the topography, while disordered regions provide fairly smooth signals.

A higher resolution image of the Si(111)$-(7 \times 7)$ domain is shown in Fig. 8 and displays almost atomic resolution in the topography (a) and in the simultaneously measured tunneling current (b). The latter signal provides higher resolution exhibiting a few visible defects, which are hardly recorded by force measurements. This proves that the tunneling current is an atomically localized effect, while the detected force is affected by the last few atoms of the tip apex.

V. CONCLUSIONS

The voltage amplifier makes it possible to choose the desired gain independent of the electric parameters of the quartz resonator and the parasitic capacitance. This leads to a better signal-to-noise ratio of the measured signal in the SFM topography acquisition. A high spring constant of an extensional-mode quartz enables a relatively fast scan with a relatively small amplitude of oscillations, which is comparable to or even lower than the characteristic short-range force decay length.

ACKNOWLEDGMENTS

This project was supported by a JARA-Start grant. The authors are indebted to Dr. D. Mayer for technical assistance in the impedance measurements and to Dr. H. J. Krause for help with the spectral noise density measurements. We also thank H. P. Bochem for the electron microscopy imaging of the sensors and the tips.

APPENDIX: QUARTZ PARAMETERS' DETERMINATION

In order to fit the theoretical impedance curve (Eq. (2)) to the experimental one the following procedure was applied. From the impedance curve, in Fig. 4, one can determine the series and parallel resonance frequencies, f_s and f_p, from the minimum and maximum, respectively, as well as the impedances at these frequencies, Z_s and Z_p. Further, at series resonance frequency f_s, the impedance Z_s is approximately equal to the motional resistance of quartz, see Eq. (4), namely,

$$Z_x \cong R_s. \tag{A1}$$

One can also estimate the impedance Z_p at the parallel resonance frequency f_p from Eq. (2), knowing that $X_0 + X_s = 0$ at $f = f_p$, namely,

$$Z_p = R_s\left[\frac{X_0^2}{R_s^2}\right] + iX_0\left[\frac{R_s^2 - X_0X_0 + X_0^2}{R_s^2}\right] = X_0\left(\frac{X_0}{R_s} + i\right). \tag{A2}$$

At the parallel resonance frequency the condition $X_0/R_s \gg 1$ is still satisfied, leading to the following expression for the impedance Z_p:

$$Z_p \cong \frac{X_0^2}{R_s}. \tag{A3}$$

Multiplying Z_s and Z_p one obtains

$$Z_sZ_p \cong X_0^2. \tag{A4}$$

Hence, the shunt capacitance C_0 can be estimated as follows:

$$C_0 = \frac{1}{2\pi f_p\sqrt{Z_sZ_p}}. \tag{A5}$$

The relation between series and parallel eigenfrequencies,[30]

$$f_p = f_s\sqrt{1 + \frac{C_s}{C_0}}, \tag{A6}$$

leads to the expression for the motional capacitance of the quartz,

$$C_s = C_0\left[\left(\frac{f_p}{f_s}\right)^2 - 1\right]. \tag{A7}$$

Finally, the motional inductance L_s can be expressed as follows:

$$L_s = \frac{1}{(2\pi f_s)^2 C_s}. \tag{A8}$$

In order to estimate the quartz electric parameters R_s, L_s, C_s as well as the shunt capacitance C_0, values of f_s, f_p, Z_s, and Z_p were read out from the particular impedance curves shown

in Fig. 4. Thereafter, using the above described recipe, the following quartz parameters were obtained: $R_s = 5042\ \Omega$, $L_s = 12.669774$ H, $C_s = 2.022065$ fF in air, and $R_s = 2501\ \Omega$, $L_s = 12.735319$ H, $C_s = 2.011591$ fF in vacuum. They are in good agreement with the values supplied by the manufacturer for the 1 MHz quartz, compared with numbers from Table I. Also the simulated curves fit the measured points very well. The value of the shunt capacitance $C_0 = 0.47$ pF was evaluated (Eq. (A5)), both in air and in vacuum. This capacitance remains in reasonable agreement with the value, which was obtained by the separate direct measurement, namely, 0.49 pF.

[1] P. Horowitz and W. Hill, *The Art of Electronics*, 2nd ed. (Cambridge University Press, Cambridge, England 1989).
[2] S. Heike and T. Hashizume, Jpn. J. Appl. Phys. **45**, 1996 (2006).
[3] T. An, T. Nishio, T. Eguchi, M. Ono, A. Nomura, K. Akiyama, and Y. Hasegawa, Rev. Sci. Instrum. **79**, 033703 (2008).
[4] F. J.Giessibl, Rev. Mod. Phys. **75**, 949 (2003).
[5] K. Bartzke, T. Antrack, K. H. Schmidt, E. Dammann, and Ch. Schatterny, Int. J. Optoelectron. **8**, 669 (1993).
[6] U. Grunewald, K. Bartzke, and A. Antrack, Thin Solid Films **264**, 169 (1995).
[7] S. Heike and T. Hashizume, Appl. Phys. Lett. **83**, 3620 (2003).
[8] T. An, T. Eguchi, K. Akiyama, and Y. Hasegawa, Appl. Phys. Lett. **87**, 133114 (2005).
[9] KolibriSensor is a trademark of SPECS Surface Nano Analysis GmbH; see www.specs.com.
[10] S. Torbrügge, O. Schaff, and J. Rychen, J. Vac. Sci. Technol. B **28**, C4E12 (2010).
[11] Z. Peng and P. West, Appl. Phys. Lett. **86**, 014107 (2005).
[12] I. Morawski and B. Voigtländer, Rev. Sci. Instrum. **81**, 033703 (2010).
[13] T. R. Albrecht, P. Grütter, D. Horne, and D. Rugar, J. Appl. Phys. **69**, 668 (1991).
[14] U. Dürig, H. R. Steinauer, and N. Blanc, J. Appl. Phys. **82**, 3641 (1997).
[15] L. Nony, A. Baratoff, D. Schär, O. Pfeifer, A. Wetzel, and E. Meyer, Phys. Rev. B **74**, 235439 (2006).
[16] F. J. Giessibl, Phys. Rev. B **56**, 16010 (1997).
[17] M. Guggisberg, M. Bammerlin, Ch. Loppacher, O. Pfeiffer, A. Abdurixit, V. Barwich, R. Bennewitz, A. Baratoff, E. Meyer, and H.-J. Güntherodt, Phys. Rev. B **61**, 11151 (2000).
[18] F. J. Giessibl, Appl. Phys. Lett. **73**, 3956 (1998).
[19] H. Edwards, L. Taylor, W. Duncan, and A. J. Melmed, J. Appl. Phys. **82**, 980 (1997).
[20] J. Rychen, T. Ihn, P. Studerus, A. Herrmann, and K. Ensslin, Rev. Sci. Instrum. **70**, 2765 (1999).
[21] T. Akiyama, N. F. de Rooij, U. Staufer, M. Detterbeck, D. Braendlin, S. Waldmeier, and M. Scheidiger, Rev. Sci. Instrum. **81**, 063706 (2010).
[22] C. J. Chen, A. Schwarz, R. Wiesendanger, O. Horn, and J. Müller, Rev. Sci. Instrum. **81**, 053702 (2010).
[23] C. J. Chen, *Introduction to Scanning Tunneling Microscopy* (Oxford University Press, New York, 2008).
[24] M. Carla, L. Lanzi, E. Pallecchi, and A. Aloisi, Rev. Sci. Instrum. **75**, 497 (2004).
[25] J. Jersch, T. Maletzky, and H. Fuchs, Rev. Sci. Instrum. **77**, 083701 (2006).
[26] G. Ferrari and M. Sampietro, Rev. Sci. Instrum. **78**, 094703 (2007).
[27] D. V. Kazantsev, Instrum. Exp. Tech. **48**, 807 (2005).
[28] From Burr-Brown Products (Texas Instruments), USA; see www.ti.com.
[29] V. E. Bottom, *Introduction to Quartz Crystal Unit Design* (Van Nostrand Reinhold, New York, 1982).
[30] See www.statek.com (pdf(tn32.pdf for STATEK Corporation, Technical Note 32.
[31] See www.statek.com for data from STATEK Corporation, USA.
[32] P. R. Gray, P. J. Hurst, S. H. Lewis, and R. G. Meyer, *Analysis and Design of Analog Integrated Circuits*, 4th ed. (Wiley, New York, 2001).
[33] B. Parzen, *Design of Crystal and Other Harmonic Oscillators* (Wiley, New York, 1983).
[34] H. W. Ott, *Noise Reduction Techniques in Electronic Systems* (Wiley, New York, 1976).
[35] C. D. Motchenbacher and J. A. Connelly, *Low-Noise Electronic System Design* (Wiley-Interscience, New York, 1993).
[36] See www.nanosurf.com for Nanosurf AG, Switzerland.
[37] See www.specs.com for SPECS Surface Nano Analysis GmbH.
[38] See www.femto.de for FEMTO Messtechnik GmbH.
[39] K. Kobayashi, H. Yamada, and K. Matsushige, Rev. Sci. Instrum. **80**, 043708 (2009).
[40] G. H. Simon, M. Heyde, and H.-P. Rust, Nanotechnology **18**, 255503 (2007).